High-Temperature, Short-Time Sulfation of Calcium-Based Sorbents. 2. Experimental Data and Theoretical Model Predictions

Corey R. Milne, Geoffrey D. Silcox,* and David W. Pershing

Department of Chemical Engineering, The University of Utah, Salt Lake City, Utah 84112

David A. Kirchgessner

Air and Energy Engineering Research Laboratory, U.S. Environmental Protection Agency, Research Triangle Park, North Carolina 27711

The fundamental processes for injection of $CaCO_3$ and $Ca(OH)_2$ for the removal of SO_2 from combustion gases of coal-fired boilers are analyzed on the basis of experimental data and a comprehensive theoretical model. Sulfation data were obtained in a 30-kW isothermal gas–particle transport reactor at conditions simulating those of upper-furnace injection. The theoretical model accounts for particle structure, calcination, sintering, sulfation, and heat and mass transfer. Pore diffusion, product-layer diffusion, and sintering appear to be the principal processes that govern the rate of SO_2 capture for the hydrate particles of interest for commercial dry sorbent injection.

Introduction

It is commonly acknowledged that SO_2 emissions from coal-fired boilers are a major contributor to the acid rain dilemma. Dry sorbent injection is a potentially attractive retrofit technology for the reduction of these emissions. In this process, $CaCO_3$ (referred to as carbonate) or $Ca(OH)_2$ (referred to as hydrate) is injected into the post-flame zone of the boiler in the radiant section. The sorbent rapidly calcines to produce CaO, which subsequently reacts with available SO_2 according to the reaction

$$CaO(s) + SO_2(g) + \tfrac{1}{2}O_2(g) \rightarrow CaSO_4(s) \qquad (1)$$

The primary advantages of pulverized dry sorbent addition over conventional wet scrubbing for SO_2 control are its lower cost, the ease with which it can be retrofitted to existing boilers, the attractiveness of a dry product, and the reduced space requirements. The primary disadvantages of this process are the low calcium-utilization efficiencies and the potential of increased fouling of heat-exchange surfaces.

Direct sorbent injection for SO_2 control was the focus of a research program launched by the U.S. Public Health Service (an EPA predecessor) in 1964. Since that time, numerous funamental, pilot- and full-scale tests have been performed on various aspects of this concept. Early fundamental work by Borgwardt (1970) and Ishihara (1970) indicated that intraparticle resistances dominated below approximately 50 μm. Hartman and Coughlin (1976) subsequently demonstrated that the overall rate of sulfation was controlled by internal diffusion for particles larger than 0.1 mm at temperatures around 1200 K. Recent

*Author to whom all correspondence should be addressed.

0888-5885/90/2629-2201$02.50/0

results by Borgwardt and Bruce (1986) indicated that, under typical boiler conditions with 1-μm particles, the dominant resistance was that of product-layer diffusion.

Pilot- and full-scale testing have emphasized the practical application of the process. Early investigations (Coutant et al., 1971; Attig and Sedor, 1970) indicated that maximum limestone utilizations were less than 20% and that the optimum sorbent injection temperature was approximately 1340 K.

Recent fundamental and pilot-scale results have considerably enhanced the overall understanding of the sorbent injection process, although they are in general agreement with the early data regarding the poor utilization that can be expected with limestone under realistic boiler conditions. Overmoe et al. (1985) measured calcium utilizations of 10–20% with limestone. They also found that hydrated limes gave significantly higher SO_2 capture. Similar results have been reported by Bortz and Flament (1985), Beittel et al. (1985), and Slaughter et al. (1985). Silcox et al. (1987) have recently reported time-resolved data (>0.1 s) that suggest that the initial sulfur capture with hydrates, and to a lesser extent carbonates, is extremely rapid and that subsequent capture is relatively slow.

Bortz and Flament (1985) measured the calcination rate of hydrates to be dramatically higher than that of carbonates. Their data indicate that the rate of calcination should impede sulfation in the early stages of reaction. Gullett and Blom (1987) reported a strong dependence on particle size for both hydrate and carbonate capture at 1373 K. Gullett and Bruce (1987) have examined the pore structure of low-temperature (1073 K) CaO prepared from both carbonates and hydrates; they determined that, with CaO prepared from carbonate materials (c-CaO), the pores approximate cylinders, while materials from hydrates (h-CaO) have pores that approximate slits.

The strong dependence of reaction rate on initial CaO surface area, reported by Borgwardt and Bruce (1986), suggests that the calcination and subsequent sintering processes are of major importance in the overall reactivity of the sorbent because these processes determine sorbent surface area. The recent work of Borgwardt (1989) showed that sintering rate is complicated by a dependence on CO_2 and H_2O concentration in the combustion gas.

Silcox et al. (1987) emphasized the importance of reactor design by showing that short-time hydrate sulfation in an isothermal bench-scale reactor was extremely sensitive to the mixing conditions after sorbent injection.

Thus, the measured sulfur capture in bench- or pilot-scale reactors at upper-furnace conditions is the result of a host of competing and complementary processes. Thorough analysis of such data necessitates the application of mathematical models that account for the simultaneous processes.

The objective of this study was to experimentally characterize the sulfation of sized and raw sorbents under the high-temperature, short-time conditions typical of injection in coal-fired boilers. A 30-kW refractory-walled flow reactor was used to obtain isothermal SO_2 capture data. A theoretical model developed by Milne et al. (1990a,b) was employed to analyze these data. In addition, the sensitivity of the various model parameters at dry sorbent injection conditions was evaluated.

Experimental Facilities

Reactor. The sulfation experiments were conducted in the dispersed-phase isothermal reactor shown in Figure 1. Natural gas, doped with SO_2, was burned to provide an appropriate combustion environment for the SO_2/CaO

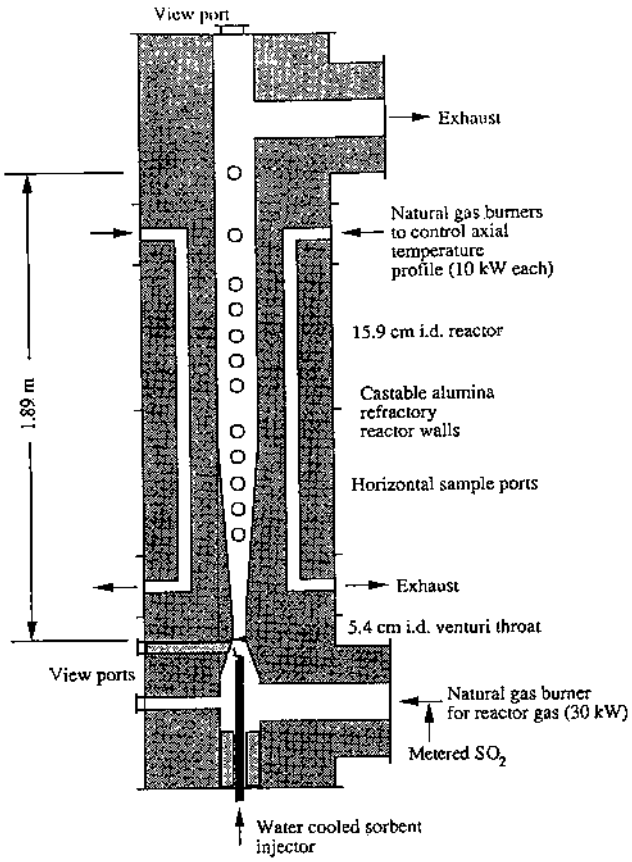

Figure 1. Dispersed-phase isothermal reactor for sulfation rate measurements.

reaction. A primary firing rate of 30 kW was used to provide the 1367 K, 5% O_2 (dry basis) conditions required for this study. The high-alumina refractory walls were cast to provide a 15.9-cm inside diameter. A venturi with a 5.4-cm-i.d. throat was located at the point of sorbent injection to ensure turbulent flow during initial sorbent mixing and to facilitate the measurement of sulfation extent at short times. The reactor was maintained under isothermal conditions (±11 K) over the length of the first 11 sample ports by the countercurrent auxiliary heating channels that were fired at a nominal rate of 20 kW. Because the final sample port was beyond the auxiliary firing channels, the gas temperature dropped approximately 17 K. Temperature was measured with a suction pyrometer employing a Type-R thermocouple.

All air flows were monitored with calibrated rotameters; natural gas was metered with a dry gas meter. The overall furnace material balance using the O_2 and CO_2 concentrations measured in the exhaust was routinely within ±3% based on an average natural gas composition.

The sorbent feed rate was metered with a K-tron T-20 twin-screw feeder that was mounted on a Sartorius 30-kg electronic balance with an accuracy of ±0.1 g. The balance output was continuously recorded for calculation of the sorbent feed rate; the typical feed rate for a hydrate was 7 g/min. A uniform sorbent feed rate, which was particularly difficult to maintain with hydrates, was achieved by entraining the sorbent in a high-velocity flow, approximately 28 m/s, past the screw tips. A low-clearance mixing block was machined to fit on the end of the screw housing with a 4.6-mm-i.d. flow channel directed perpendicular to the screw axes and between the twin screws; the screw tips extended beyond the screw housing by 2 mm.

The sorbent was transported from the feeder to the injection point in the reactor with dry nitrogen. Dispersion

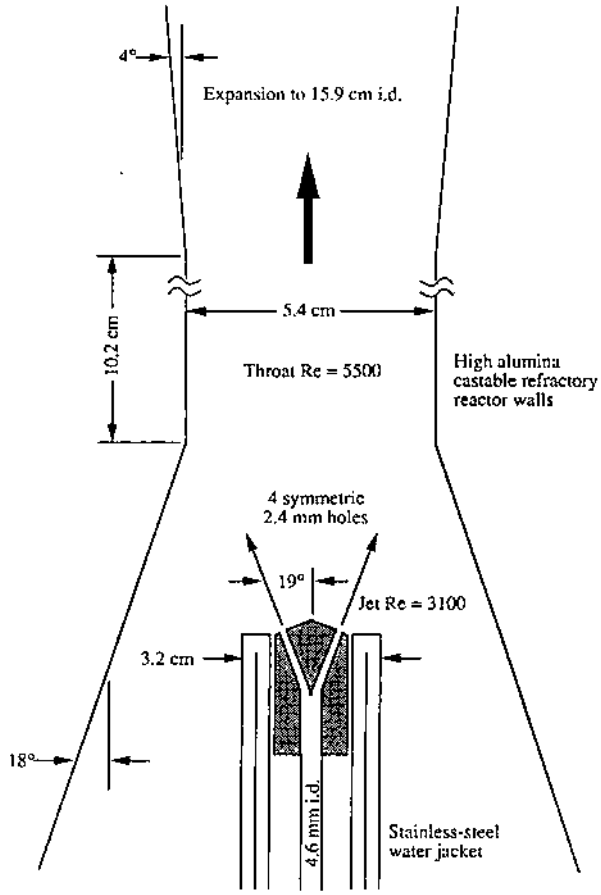

Figure 2. Schematic diagram of injector and reactor venturi.

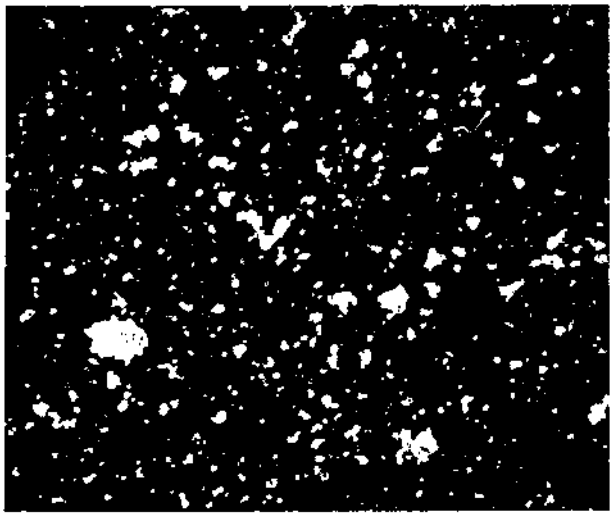

Figure 3. SEM photomicrograph showing the extent of agglomeration of raw Linwood hydrate, with a 2.5-μm mass mean diameter, after injection at 1367 K (0.38 cm = 15 μm).

was accomplished with a four-hole nozzle at the tip of a water-cooled probe. Both solid distribution and tracer tests were conducted to ensure that the divergent nozzle injecting into the throat of the reactor venturi (see Figure 2) produced rapid, uniform mixing. Addition of SO_2 with the sorbent injected into the reactor instead of blending the SO_2 at the natural gas burner did not result in a different level of sulfur capture, implying that SO_2 in the reactor gas stream was rapidly contacted with the injected sorbent.

Gullett and Blom (1987) reported that Linwood hydrate injected at 1373 K showed significant agglomeration of the

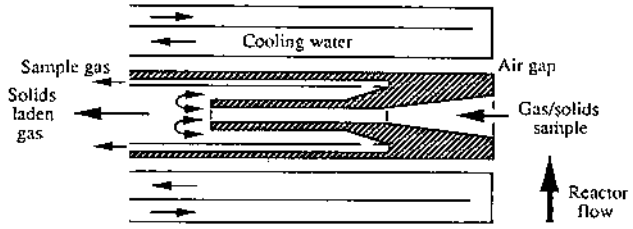

Figure 4. Phase discrimination tip of gas sample probe.

individual particles. Figure 3 shows a SEM photomicrograph of Linwood hydrate injected at 1367 K collected on a SEM sample stub by the procedure outlined by Milne et al. (1990b). The sampling procedure has an inherent selectivity for larger particles due to inertial flow effects. The photomicrograph shows some 10-μm agglomerates or particles as well as many approximately 2-μm particles; the mass mean diameter of the sorbent is 2.5 μm. Thus, agglomeration after injection does not appear to significantly increase the effective particle size.

Gas Sampling. SO_2 concentration measurements were obtained with a Du Pont Model 400 nondispersive ultraviolet analyzer. The instrument output was read on a chart recorder concurrently with the weight of the sorbent feeder. The reactor gas was drawn by inserting a stainless steel water-cooled sample probe in 1 of the 12 radial side ports. The port nearest the sorbent injector was equivalent to a reaction time of 0.04 s, assuming plug flow of the reactor gas; port 12, 1.9 m from the sorbent injection point, corresponded to a residence time of 0.5 s.

Figure 4 illustrates the phase-discrimination tip of the SO_2 sample probe which was designed to minimize gas/solid reactions after sampling. The sample gas was drawn from the reactor through a high-velocity water-cooled nozzle to (1) rapidly separate the majority of the solids from the sample gas stream through a high-velocity 180° turn and (2) quickly quench further reaction of the solids remaining in the sample stream without condensing sulfuric acid. The sample gas passed from the probe through a heated line to a Perma-pure membrane dryer where essentially all of the water vapor was removed prior to measurement by the continuous NDUV SO_2 analyzer. Initial testing indicated that, in the most extreme case (smallest, most reactive sorbent particles), the phase discrimination tip was capable of reducing probe capture to less than 2% at Ca/S = 2. Replicated sorbent injection tests over the period of this study have indicated that the sulfur capture measurements at 0.5 s are reproducible to within ±2.5%; this spread increases to ±5% for the more difficult 0.04-s measurements.

Sized Sorbents. To investigate the influence of particle size, 34-kg batches of hydrate and carbonate sorbents were sized in a Vortec Model C-1 air classifier to produce four size cuts. The influence of parent rock source, which can be significant according to Boynton (1980), was minimized by acquiring both the hydrate and carbonate from the same source, the Linwood Mining and Minerals Corporation of Davenport, IA. The hydrate was, therefore, directly derived from the carbonate using normal, atmospheric pressure hydration techniques. The sized sorbents were subsequently analyzed by mechanical sieving and by X-ray sedimentation with a Micromeritics Sedigraph analyzer. These results are summarized in Table I. The Sedigraph yields the equivalent spherical diameter of a particle with the same true density as the actual particles based on Stoke's law settling rates. While these particle size data are believed to indicate the particle size distribution that actually existed within the isothermal furnace, note that

Table I. Particle Size Analysis of Sized Linwood Hydrate and Carbonate

sorbent	specified cut size, μm	cut amt, wt %	mass mean diameter, μm	size range for 90% of particles, μm	content of Ca, %	solids density, g/cm³
$Ca(OH)_2$	no cut	100	2.5	0.8–19	49.5	2.248
$Ca(OH)_2$	<3	26.0	1.9	0.6–3.1	48.6	2.249
$Ca(OH)_2$	3–7	64.4	2.4	1.1–7.0	49.4	2.206
$Ca(OH)_2$	7–20	2.4	5.4	0.9–11	47.0	2.305
$Ca(OH)_2$	>20	7.2	42	5.0–200	42.9	2.463
$CaCO_3$	no cut	100	25	4.1–100	35.9	2.713
$CaCO_3$	3–7	8.7	4.4	2.2–8.0	34.9	2.705
$CaCO_3$	7–20	21.2	8.9	4.3–17	35.9	[a]
$CaCO_3$	20–40	23.8	21	12–33	36.4	[a]
$CaCO_3$	>40	46.3	54	27–120	36.6	2.723

[a] Not determined.

the accuracy of the data is limited by the assumptions inherent in the Sedigraph measurement, particularly the assumption that the particles are spherical when in fact they are quite angular.

The agglomeration of hydrate materials reported by Gullett and Blom (1987) is substantiated by the fact that, in the case of the hydrated sorbent of Table I, the particle size as measured by the Sedigraph is significantly smaller than that inferred from the air classification cut.

The calcium content of the sorbent was determined by acid digestion and EDTA titration. The density of the solids was measured by helium displacement with a Micromeritics Autopycnometer.

Sulfation Model

The elements of a comprehensive sulfation model that incorporates calcination, sintering, intrinsic sulfation, particle swelling, pore filling, external mass transfer, pore diffusion, and product-layer diffusion were developed by Milne et al. (1990a,b). The structural model is based on the concept of overlapping spheres introduced by Lindner and Simonsson (1981). This comprehensive model is the result of an effort to account for the multitude of simultaneous processes that occur during dry sorbent injection in a combustion gas containing SO_2. Fundamental data were inadequate in many instances to completely define the governing principles. Rather than ignore these areas of uncertainty, assumptions consistent with the structural model and available literature data have been incorporated in the model.

Briefly, the model views the calcining sorbent particle as a shrinking core of unreacted material. Each shell of product CaO is modeled as a matrix of high surface area, overlapping spherical grains that subsequently sinter and react with SO_2. The rate of sulfation is limited by product-layer diffusion, which is influenced by surface area, grain overlap, and product-layer thickness. Sulfation is also limited by gas-phase diffusion to the particle surface and pore diffusion through the particle, which is dependent on porosity and mean pore diameter. The rate of calcination, which limits the rate at which CaO is available for reaction, is a function of sorbent type and particle diameter. The rate of sintering is a function of the concentration of CO_2 and H_2O in the gas phase and the surface area of the CaO grains. The required rate expressions were determined from the available fundamental literature as described in part 1 of this paper (Milne et al., 1990b); no adjustments were made to improve the agreement with the experimental results of this study.

The rates of all these processes are increased by higher temperatures. In general, models for the sulfation of calcium-based sorbents assume isothermal conditions. Because the rate of heat transfer is dependent on particle size and the reaction rates are rapid enough that heat-transfer limitations could impede the overall sulfation process, heat transfer is incorporated in the sulfation model.

Heat Transfer. To account for the possible influence of high mass-transfer rates due to calcination, the film theory development of Bird et al. (1960) was used by Milne et al. (1990b) to determine the external SO_2 mass-transfer coefficient as a function of the flux of CO_2 (or H_2O depending on the calcining sorbent), SO_2, and O_2. A similar application of the film theory yields the heat-transfer coefficient accounting for high mass-transfer rates,

$$h = \frac{k_h}{r_p}\left(\frac{\phi_h}{e^{\phi_h} - 1}\right) \tag{2}$$

where

$$\phi_h = \frac{r_p}{k_h}\sum_i F_i C_{pi} \tag{3}$$

The correction term for high mass-transfer rates, the term in parentheses in eq 2, reduces to unity for the limit of zero flux. The term k_h is the thermal conductivity of the gas mixture evaluated at film conditions (average of the particle and gas temperatures). For the combustion gas mixtures of this study (4.3% O_2, 7.5% CO_2, 14% H_2O, and the balance N_2), eq 4 is used to evaluate k_h:

$$k_h = (5.49 + 0.0641T)10^{-3} \tag{4}$$

The thermal conductivities of O_2, CO_2, and N_2 are very similar. Equation 4 is a correlation of values calculated from the predictive gas mixture thermal conductivity equation of Gambill (1973) and the thermal conductivity data for individual gases from Liley (1984).

A heat balance accounting for radiation, convection, mass transfer between the particle and the bulk gas, and heat of reaction results in a nonlinear differential equation. A finite difference approach and evaluation of the nonlinear radiation term based on the particle temperature from the previous time step yields an explicit method for evaluating the change in temperature for small time steps,

$$T_p = (\sigma\epsilon(T_w^4 - T_{p1}^4) + hT_g + \alpha T_{p1} - \sum_i F_i C_{pi}(T_1 - 298) - \sum_j |F_j|\Delta H_{rj})/(h + \alpha) \tag{5}$$

where h is determined with eq 2 and

$$\alpha = \frac{n_{Ca}}{4\pi r_p^2 \Delta t}\{(1 - x_c)C_{p1} + x_c[(1 - x_s)C_{p2} + x_s C_{p3}]\} \tag{6}$$

The emissivity of CaO is 0.27 (Satterfield and Feakes, 1959). The flux term, F_i, is positive for flux away from the particle. Subscript i refers to the gas species SO_2, O_2, and

Table II. Coefficients for Mean Heat Capacities of Gases and Heat Capacities of Solids

species (i)	a_i	$10^3 b_i$	$10^6 c_i$	$10^{10} d_i$	$10^{-5} e_i$	range, K
SO_2[a]	7.903	6.332	−3.131	6.117	0	298–1473
O_2[a]	6.701	0.9718	0.2275	−1.739	0	298–1473
CO_2[a]	7.105	6.896	−3.296	6.678	0	298–1473
H_2O[a]	7.936	−0.1195	1.500	−4.650	0	298–1473
$CaCO_3$[b]	24.98	5.24	0	0	−6.20	298–1473
$Ca(OH)_2$[c]	21.4	0	0	0	0	276–373
CaO[b]	11.67	1.08	0	0	−1.56	298–1800
$CaSO_4$[b]	18.52	21.97	0	0	−1.57	273–1373

[a] Correlation of the tabulated values in Hougen et al. (1954). [b] Coefficients reported in Balzhiser et al. (1972). [c] Heat capacity reported by Liley (1984).

Table III. Coefficients for Heat of Reaction

reaction	a_i	$10^3 b_i$	$10^6 c_i$
$CaCO_3$ calcination	43.1	−1.520	−1.257
$Ca(OH)_2$ calcination	26.1	0	0
CaO sulfation	−119.5	−1.230	2.203

CO_2 or H_2O, depending on the sorbent type. Subscript j refers to the heat of reaction and the gaseous products, CO_2 or H_2O for calcination and SO_2 and O_2 for sulfation. The term n_{Ca} is the moles of Ca in the particle, and subscripts 1, 2, and 3 differentiate between the molar heat capacities of the sorbent [$CaCO_3$ or $Ca(OH)_2$], CaO, and $CaSO_4$, respectively. Internal temperature gradients are negligible based on the fact that the Biot number for the particles of interest is less than 0.1 (Holman, 1976).

Table II lists the coefficients of the mean heat capacities of the gases of interest with a reference temperature of 298 K. Also listed are the coefficients for the heat capacities of the solids of interest for sorbent injection. The coefficients of Table II are substituted in eq 7 to determine the heat capacity C_{pi} (J/(kmol K))

$$C_{pi} = 4187(a_i + b_i T + c_i T^2 + d_i T^3 + e_i/T^2) \quad (7)$$

Based on the heats of reaction at 298 K [42.5 kcal/mol for carbonate calcination, 26.1 kcal/mol for hydrate calcination, and −120 kcal/mol for sulfation of CaO (Hougen et al., 1954)] and the heat capacities calculated from Table II, the heats of reaction at various temperatures were calculated and fit with the quadratic equation

$$\Delta H_{ri} = 4.187 \times 10^6(a_i + b_i T + c_i T^2) \quad (8)$$

to obtain the coefficients in Table III for evaluating the heat of reaction at temperatures up to 1500 K.

Discussion of the Experimental Results

Experimental Conditions. The base experimental conditions around which parametric studies were performed were 148 Pa SO_2 (2000 ppm SO_2, dry basis), 3.7 kPa O_2, 6.5 kPa CO_2, 12.1 kPa H_2O, 63.8 kPa N_2, 1367 K, Ca/S = 2, and reaction times of 0.04–0.55 s. Unless otherwise specified, the data and model predictions of this paper are based on these conditions. The reactor was operated at essentially atmospheric pressure, 86.1 kPa.

Precalcines. Theoretical sulfation models are typically compared to reactor data by conducting sulfation measurements with precalcined CaO of known pore structure to eliminate the uncertainties induced by the calcination step and provide a structural basis for pore-diffusion calculations. Model predictions in Figure 5 for sulfation of a precalcine injected in the isothermal reactor at 1367 K show much less capture than actual measurements. A basic premise of the model is that the sorbent pore structure is not altered by the flash heating that takes place upon injection.

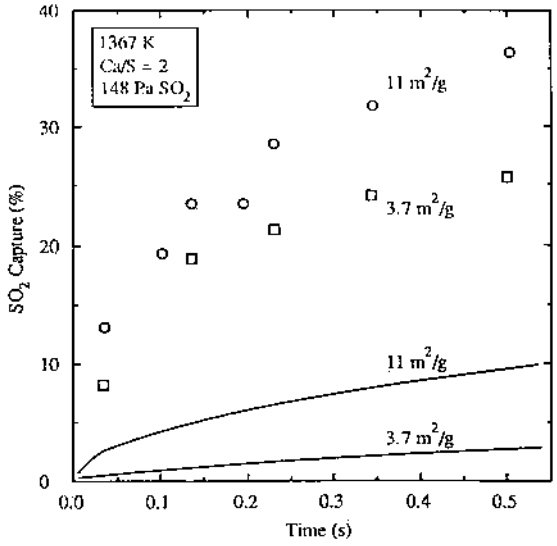

Figure 5. Sulfur capture data (symbols) for 7-μm Linwood c-CaO compared with model predictions (lines).

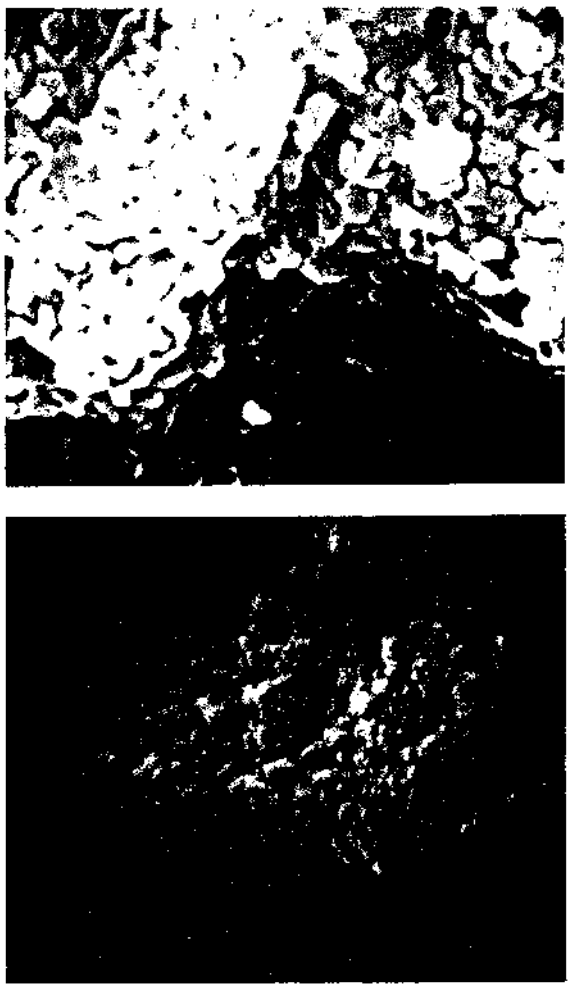

Figure 6. SEM photomicrographs of 11 m^2/g CaO derived from 8.9-μm Linwood carbonate: (a) before injection and (b) 0.04 s after injection in 1367 K flow reactor without SO_2 (2.8 cm = 7.0 μm).

SEM photomicrographs are displayed in Figure 6 that show the before and after injection structures of the 11 m^2/g c-CaO that was employed to obtain the data of Figure 5. The marked contrast between the two structures, smaller grains with an associated higher surface area exhibited in Figure 6b relative to that in Figure 6a, indicates that flash heating to 1367 K, by the rapid mixing system

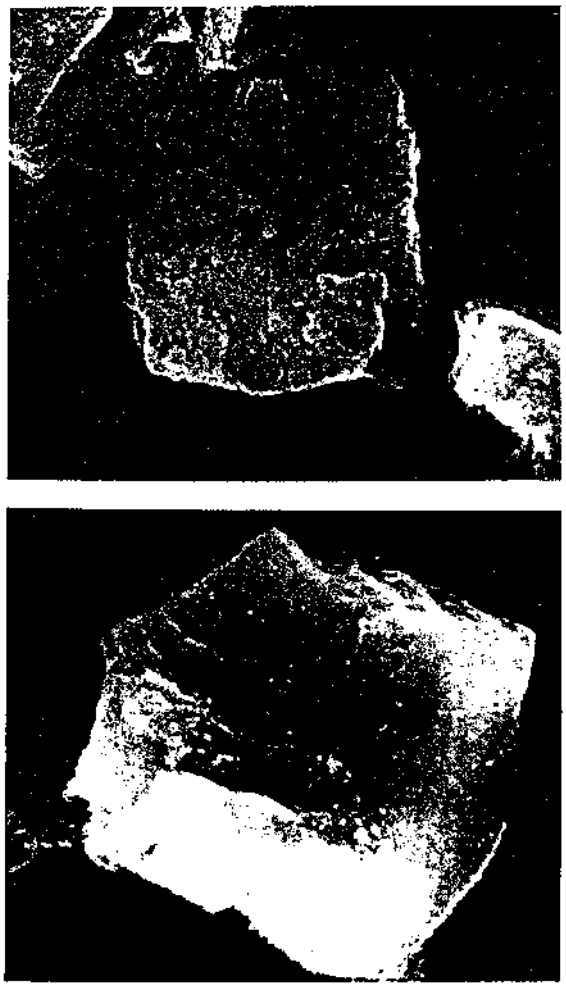

Figure 7. SEM photomicrographs of 11 m^2/g CaO derived from 8.9-μm Linwood carbonate: (a) before injection and (b) 0.04 s after injection in 1367 K flow reactor without SO_2 (3.85 cm = 10 μm).

of the reactor for this investigation (Figure 2), significantly altered the CaO structure. Note that all of the photomicrographs presented are representative of the entire sample deposited on the SEM sample stub.

Silcox et al. (1987) measured particle fragmentation for $CaCO_3$ calcined at 1633 K, but they postulated that fragmentation is negligible at the temperatures of interest for dry sorbent injection. In agreement with their findings, Figure 7 shows lower magnification SEM photomicrographs of the Figure 6 particles, before and after injection, with no evident fragmentation.

The precalcines for this study were produced by decomposition at 1073 K for 45 min with a bed depth of 5 mm in a ceramic pan set in an air-purged electric muffle furnace. An additional 15 h in the furnace reduced the surface area from 11 to 3.7 m^2/g but did not result in additional decomposition, based on weight loss and Ca weight percent. A possible explanation for the altered structure after injection is that a small amount of $CaCO_3$ remained in the interior of the particle grains due to diffusion limitations. The flash heating resulted in a high CO_2 vapor pressure at these sites of residual $CaCO_3$. Calcination proceeded by fracturing of the grains to release CO_2, resulting in a decrease in grain size, exhibited in Figure 6b. The resulting higher surface area and porosity attributed to this explanation should bring the model predictions in line with the sulfation data of Figure 5. Similar disparities between precalcine data and model predictions were observed for all sizes of hydrate- and carbonate-derived CaO.

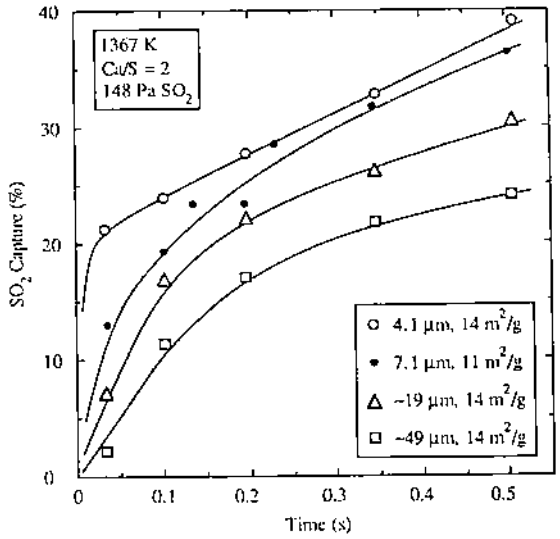

Figure 8. Sulfation data for sized Linwood c-CaO with similar preinjection surface areas.

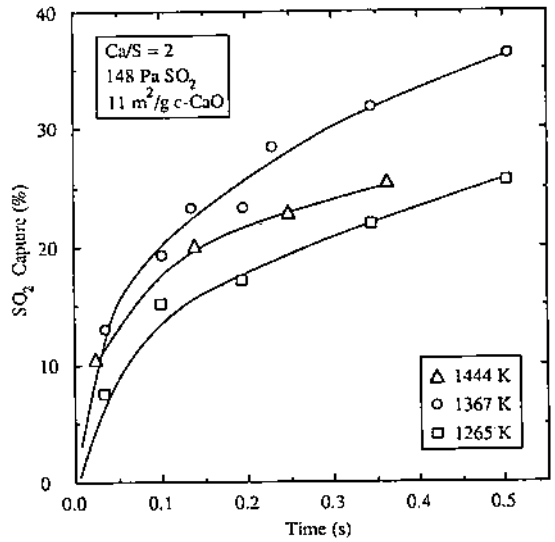

Figure 9. Sulfur capture data for 7-μm Linwood c-CaO showing the influence of reactor temperature.

Therefore, the precalcine sulfation data obtained in this study cannot be rigorously applied for model development due to uncertainty of the post-injection porosity and surface area. However, these data, which do not have the complication of simultaneous calcination, are of value for quantifying relative changes in sulfation rate induced by variations in temperature, particle size, Ca/S molar ratio, and SO_2 partial pressure.

Sulfur capture data for sized precalcines, plotted in Figure 8, show that initial capture is a strong function of particle diameter, but the parallel nature of the capture curves after 0.2 s suggests that subsequent sulfation is relatively insensitive to particle size. The fact that the largest particle size exhibits a much slower, more monotonic increase in sulfur capture with reaction time implies that the initial sulfation rate is being retarded by internal pore diffusion. For times greater than 0.2 s, the nearly parallel lines could result from product-layer-diffusion control. Thus, the difference in capture at 0.2 s probably reflects the loss of calcium sites (specifically microporosity) due to catalyzed thermal sintering during the period in which sulfation is being retarded by internal pore diffusion.

The precalcine data for different temperatures, Figure 9, suggest an optimum of 1400 K for isothermal sulfation

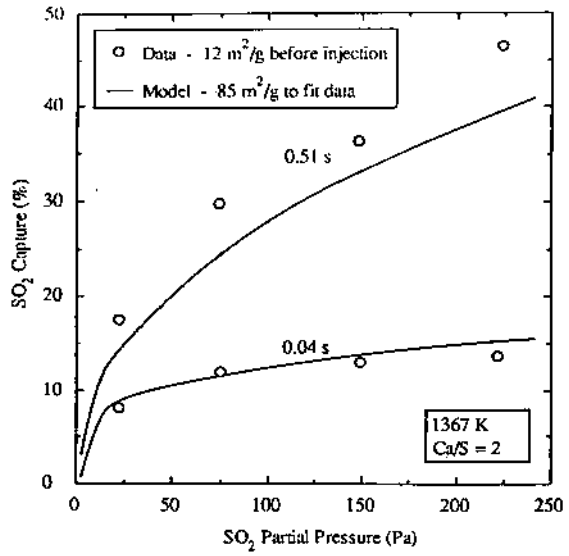

Figure 10. Concentration dependence of 7-μm Linwood c-CaO sulfur capture: experimental data and model predictions with a fitted surface area.

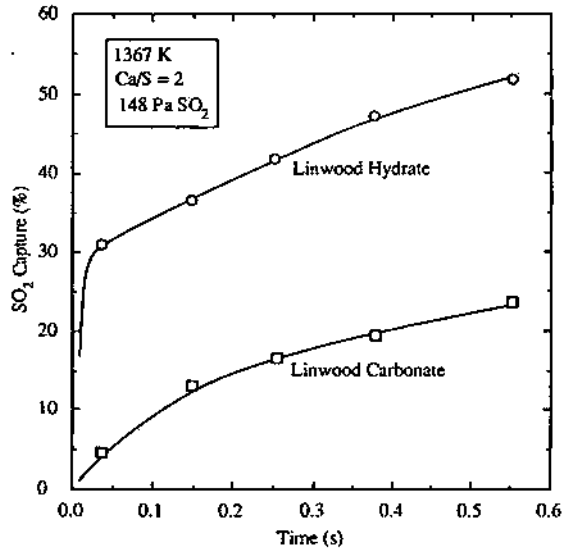

Figure 11. Sulfur-capture data for commercially available Linwood hydrate and carbonate.

of CaO. The data show that early capture, at times less than 0.05 s, increases with temperature, but for longer times, >0.05 s, there is a reduced rate of capture for the higher temperatures.

The dependence on SO_2 partial pressure is illustrated in Figure 10. To compare predicted and actual concentration related trends, a model surface area of 85 m^2/g was employed to bring the predicted level of capture in line with the 12 m^2/g CaO sulfation data. Though the precalcine sulfation data do not serve as the basis for calibrating the pore structure related features of the model, the data do lend assurance that the model represents trends related to changes in SO_2 partial pressure.

The weaker dependence on SO_2 concentration of the 0.04-s model predictions is due to the model assumption that initial monolayer coverage of the CaO surface with $CaSO_4$ is instantaneous, limited only by gas-phase diffusion. The subsequent 0.6-order dependence, invoked after monolayer coverage, results in the stronger influence of concentration for the 0.51-s model predictions.

Commercial Materials. The initial experimental studies were conducted with raw, commercial sorbents to characterize reactivity differences that would be expected

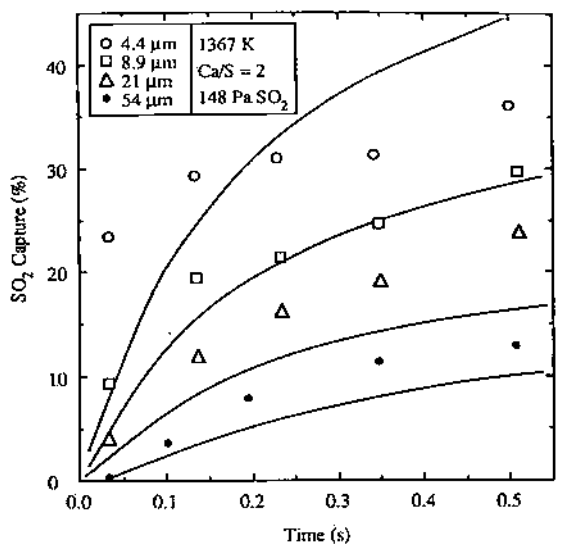

Figure 12. Influence of particle size on sulfation of Linwood carbonate: model predictions compared with experimental data.

in a large-scale industrial application. Figure 11 illustrates the time-resolved SO_2 capture data obtained for the Linwood carbonate and the hydrate commercially produced from the carbonate. As observed previously by numerous other investigators (Bortz and Flament, 1985; Beittel et al., 1985; Overmoe et al., 1985), the ultimate SO_2 capture with the hydrated sorbent significantly exceeds that obtained with the limestone. However, the time-resolved data shown in Figure 11 indicate that this difference is primarily due to a dramatic difference in initial sorbent reactivity. For the hydrated sorbent, the sulfur capture at 0.04 s accounts for approximately 60% of the 0.55-s capture; in contrast, the initial limestone capture represents only 20% of that ultimately achieved. After 0.15 s, the slopes of the two curves are surprisingly similar.

The large reactivity differences exhibited by hydrate and carbonate sorbents are attributed to three inherent differences in the sorbents. First, both sorbents must calcine to produce CaO prior to reaction with SO_2; however, the carbonate sorbent calcines significantly more slowly than the hydrate. Calculations using the activation model of Milne et al. (1990a) suggest that the mean size hydrate particles calcine in less than 0.01 s under the conditions of this experiment, while the mean carbonate particles require in excess of 0.3 s to fully calcine. The second potentially important factor is a difference in the structure of the CaO produced. Gullett and Bruce (1987) have suggested that c-CaO has internal pores that can be reasonably approximated by cylinders while h-CaO appears to have slit- or platelike structures. The third and final difference is the characteristic particle size distribution of the commercial materials. Gullett and Blom (1987) reported that hydration of CaO produced from $CaCO_3$ reduced the mean particle diameter by over 80% relative to the parent carbonate. A similar size reduction in the commercial hydration process results in a mass mean diameter of 2.5 μm for Linwood hydrate, compared to the 25-μm mass mean size of Linwood carbonate.

Influence of Particle Size. Figure 12 shows the time-resolved capture results for the four particle classes of the carbonate sorbent. Characteristics of the different size fractions are listed in Table I. As seen with the precalcine data of Figure 8, these data show that the initial sulfation rate is strongly influenced by the mean particle size but the rate after 0.2 s is essentially independent of size. The chemical analyses of the sized carbonates, shown

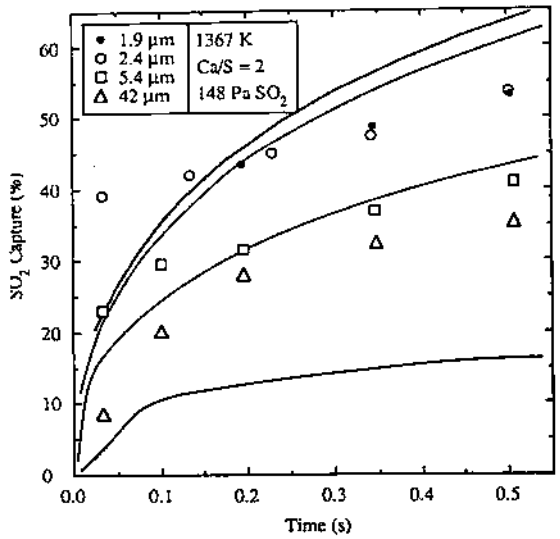

Figure 13. Influence of particle size on sulfation of Linwood hydrate: model predictions compared with experimental data.

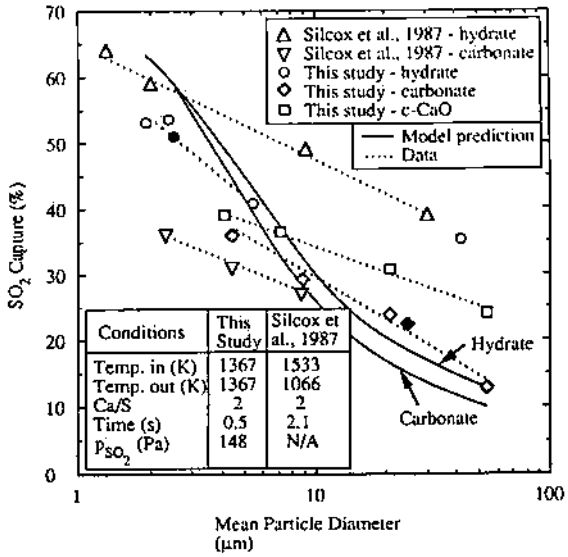

Figure 14. Sulfur capture as a function of particle diameter for Linwood hydrate and carbonate. Model predictions and experimental data from this study are compared with data from Silcox et al. (1987).

in Table I, indicate little chemical difference among the size groups. This uniformity is confirmed by the true density measurements.

The apparent delay prior to the onset of sulfation exhibited by the largest carbonate particles is associated with pore diffusion and with the time required for significant calcination to occur. The sulfation data of the commercial limestone with a mean mass particle size of 25 μm, Figure 11, are in good agreement with the 21-μm narrow size cut of Figure 12. The relatively small amount of prompt capture exhibited by the unsized material is consistent with the data obtained using the various size fractions; the raw sorbent only contains about 9% of the small particles (4.4 μm) that are capable of producing large amounts of initial sulfur capture.

Model predictions for various size carbonate particles, Figure 12, imply a stronger particle size dependence for 0.5-s capture than the data support. In contrast, the predicted particle size influence on prompt capture falls short of measured quantities. Apparently the model assumption of instantaneous monolayer sulfation along with the gas-phase diffusion limitations does not adequately simulate the actual process. Though the model predicts subsequent levels of capture similar to the data, the near-parallel capture curves after 0.2 s inferred from the data are not predicted. Model calculations predict a transition from pore diffusion dominance for the 21- and 54-μm particles, to a combined pore-diffusion and product-layer-diffusion limited case for the two smaller particles. The hypothesis that the parallel nature of the capture data curves after 0.2 s is evidence of product-layer-diffusion control is not supported by the model, which predicts strong pore-diffusional limitations down to approximately 1 μm.

The time-resolved sulfur capture data for the sized hydrates, shown in Figure 13, exhibit the same general dependence on particle size. The prompt capture (39% at 0.04 s) with the 2-μm particles indicates that the initial calcination and sulfation of small hydrate particles is extremely rapid relative to the subsequent sulfation rate. In agreement with the data, the model predicts little difference between the 1.9- and 2.4-μm capture curves. The hydrate model predictions show the same type of variance with the data as observed with the carbonate.

It should be noted that the calcium content of the largest size cut (42.9%) is significantly less than the 49 wt % calcium of the two smallest size fractions. This suggests that the largest cut (and to a lesser extent the 5.4-μm cut) contained inert contaminants. Physically these large contaminants appeared gray and were inert to HCl, suggesting that they did not contain calcium carbonate. It is therefore likely that the largest particles in this cut were relatively inert with respect to SO_2 sorption. Consequently, the 42-μm hydrate material is of doubtful value in evaluating the influence of particle size. Model predictions of much lower capture levels for 42-μm hydrate particles support this contention.

The unsized Linwood hydrate sorbent of Figure 11, dominated by small particles with a mass mean size of 2.5 μm, shows slightly lower capture than the narrow size distribution 2.4-μm hydrate of Figure 13.

For both hydrates and carbonates, the level of prompt capture for small particles is not accurately predicted by the model, and the particle size dependence for subsequent capture is overestimated. The fact that initial hydrate capture predictions are much lower than actual prompt capture suggests that calcination rate is not a factor in the inadequacy of the model; rather, the failure is primarily related to the pore-diffusion aspects of the model.

The hydrates of Figure 13 show much higher levels of capture than the carbonates of Figure 12, due mainly to the particle size differences. Figure 14 provides direct comparison of these data at a reaction time of 0.5 s. Figure 14 includes data obtained by Silcox and co-workers (1987) using aerodynamically sized particles with the same two Linwood sorbents. These data represent exhaust measurements from a bench-scale furnace with a decaying thermal profile that simulates a full-scale boiler. Although these results are not directly comparable (isothermal versus decaying thermal profile), they do indicate that at long times both facilities show a similar dependence on mean particle diameter. Gullett and Blom (1987) similarly showed that the extent of sulfation is proportional to the sorbent diameter raised to the 0.3 power for particle diameters in the range 0.4–10 μm.

Model predictions included in Figure 14 show a stronger particle size dependence than exhibited by the data. The controlling mechanism in the model that produces this particle size effect is pore diffusion.

Finally, Figure 14 shows the results obtained with the unsized parent material (solid symbols), and as noted

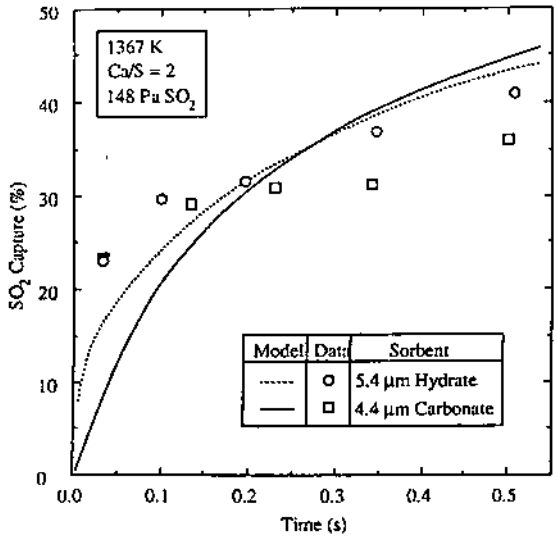

Figure 15. Sulfur capture for comparable size Linwood hydrate and carbonate particles: model predictions and experimental data.

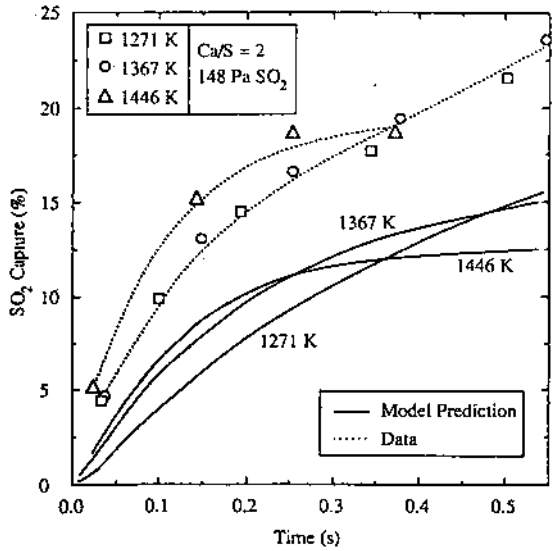

Figure 16. Sulfation of raw Linwood carbonate (25-μm diameter) as a function of temperature: model predictions compared with experimental data.

previously, these data agree well with the sized results. Thus, it appears that the major difference between the reactivity of commercial hydrates and carbonates is associated with particle size; at 0.5 s, 75% of the difference in hydrate–carbonate capture can be directly attributed to the fact that the mean size of the commercial hydrate is approximately 2.5 μm while that of the commercial carbonate is almost 25 μm. Further, this difference is largely the result of differences in prompt SO_2 capture that result from internal pore diffusion limitations during the time of peak sorbent reactivity. The flatter slope of the c-CaO data relative to the carbonate data of Figure 14 implies that carbonate calcination does increase the particle size dependence.

Influence of Calcination Rate. To more clearly address the issue of sulfation hindrance due to calcination rate, capture data for hydrate and carbonate particles of comparable sizes (approximately 5 μm) are plotted in Figure 15 along with model predictions. The actual mean size is 5.4 μm for the hydrate versus 4.4 μm for the carbonate, and the hydrate has a slightly broader particle size distribution. The calcium weight fractions, 47% versus 35%, establish that the two materials are different chemically, as expected, and that cross contamination is insignificant in either material. The weight percent of Ca in pure $Ca(OH)_2$ and $CaCO_3$ is 54% and 40%, respectively.

These data suggest that, for these small particles, the calcination rate does not retard carbonate sulfation relative to hydrate sulfation, even though the carbonate is not predicted to be fully calcined at 0.15 s, compared with the nearly instantaneous predicted calcination of the hydrate particle. These data indicate that, with small particles, the carbonate calcination delay is not of major importance and that the quantity of calcium sites initially available for reaction is similar to that for calcined hydrates. The model predictions incorrectly reveal an initial sulfation advantage of the hydrate, due to the higher calcination rate, and a minor ultimate sulfation advantage of carbonate, due to the smaller particle diameter and the interaction of sintering and calcination rates.

Influence of h-CaO and c-CaO Structural Differences. Comparison of Figures 12 and 13 reveals that, after approximately 0.2 s, the sulfation curves for both the hydrates and carbonates are similarly shaped, with the hydrate curves having a slightly steeper slope (see Figure 15). This minor difference can be attributed to structural differences inherent in the two sorbent types.

By mercury penetration techniques, the porosities of Linwood hydrate and carbonate were measured as 15% and 4%, respectively. Assuming that nonporous $CaCO_3$ and $Ca(OH)_2$ decompose to porous CaO of the same exterior volume with internal porosities of 54% and 49%, respectively, due to the differences in molar volumes of the compounds, h-CaO has an overall porosity, including the initial sorbent porosity, of 57%, and c-CaO has one of 56%.

Model predictions indicated that 2.5-μm hydrate capture at 0.5 s decreases from 60% to 53% when the initial sorbent porosity is reduced from 15% to 4%. Similar calculations for 25-μm carbonate showed an increase in capture from 15% to 17% with an increase in porosity from 4% to 15%. Therefore, the porosity of the sorbent before calcination has a substantial impact on sulfation for smaller particles where SO_2 penetration to the center of the particle is limited more by porosity than by particle diameter. In this manner, inherent structural differences in the two sorbents can account for differences in the hydrate and carbonate reactivity.

High-resolution SEM photomicrographs of hydrates and carbonates calcined at 1073 K (Milne et al., 1990a) suggest that the hypothesis of Gullett and Bruce (1987), based on CaO produced at 1073 K, is correct. The carbonate precalcine appeared to contain large numbers of interconnecting pores that could be reasonably approximated as cylinders. In marked contrast, the porosity in the hydrate precalcine had a much more angular, planar appearance. However, Milne et al. demonstrated that these striking differences in structure were not nearly as significant in h-CaO and c-CaO samples prepared by flash calcination at 1367 K. Thus, at conditions of interest for dry sorbent injection, the inherent differences in shape of h-CaO and c-CaO pores do not appear to yield significant differences in sulfur capture.

Temperature Effects. The precalcine data of Figure 9 show the influence of temperature on sulfur capture. Figures 16 and 17 show similar temperature dependence for Linwood carbonate and hydrate. The rates of calcination and gas-phase diffusion increase with temperature with a resultant increase in the rate of sulfation. The sintering rate also increases with temperature but with a reduction in the rate of sulfation. The rate of product-layer diffusion increases with temperature as the product-layer

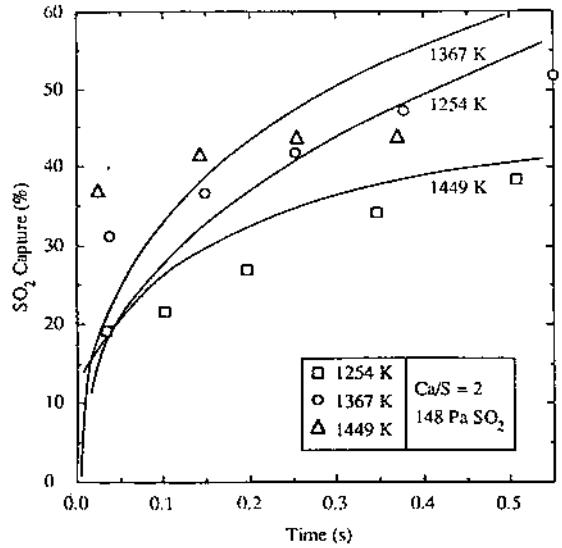

Figure 17. Temperature dependence for sulfation of raw Linwood hydrate (2.5-μm diameter): model predictions and experimental data.

diffusivity increases. Above 1400 K, the vapor pressure of $CaSO_4$ rises dramatically until eventually the vapor pressure exceeds the partial pressure of SO_2, and $CaSO_4$ decomposes. Because the rate of product-layer diffusion is proportional to the 0.6 power of the difference between the partial pressure of SO_2 and the vapor pressure of $CaSO_4$ (Milne et al., 1990b), the rate of sulfation is retarded by the higher vapor pressure of $CaSO_4$ at elevated temperatures.

The data of Figures 9, 16, and 17 with mass mean particle diameters of 7.1, 25, and 2.5 μm, respectively, show that the temperature influence is strongest with the smaller particle sizes, a point that is supported by the model predictions of Figures 16 and 17. Earlier discussions showed that the 25-μm carbonate model pedictions are dominated by pore diffusion and that calcination rate is a minor factor.

These temperature data suggest an optimum isothermal sulfation temperature of approximately 1400 K. Bortz and Flament (1985) suggest an optimum of 1370 K, and Bortz et al. (1986) suggest a higher optimum of 1450 K. Model predictions, however, indicate an optimum of 1340 K. Though the absolute value of the model prediction captures is quite different than the data values in some instances, the model does predict the trend of increasing prompt capture with temperature as well as the progressive flattening of the capture curve at longer reaction times at elevated temperatures.

Partial Pressure of SO_2. The equilibrium partial pressure SO_2 at 1445 K, 68 Pa from Reid (1970), does not appear to be the dominant factor in the flattening of the capture curves for the high-temperature hydrate and carbonate data, Figures 16 and 17. Both sets of data show no increase in capture after 0.3 s when the hydrate and carbonate have reduced the SO_2 partial pressure to 80 and 120 Pa, respectively. The model predictions, accounting for the equilibrium SO_2 concentration, show reasonable agreement with the carbonate data on the relative impact of temperature increase, but the hydrate predictions at 1449 K show a greatly reduced capture relative to the lower temperature predictions. This disagreement with the data implies that the method employed by the model of discounting sulfation rate due to high vapor pressure of $CaSO_4$ at elevated temperatures overestimates this influence.

As shown by the data of Figure 18, the influence of

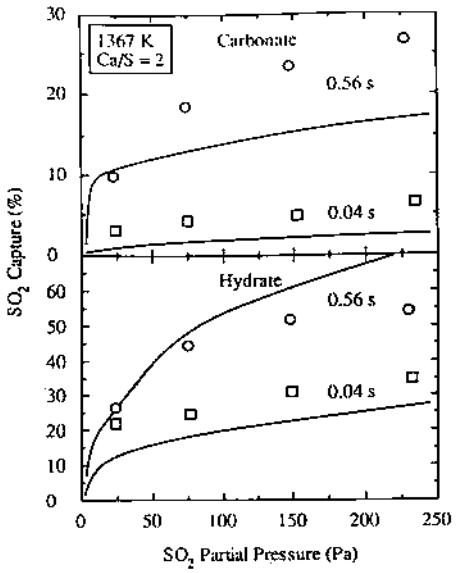

Figure 18. Influence of concentration on sulfur capture for raw Linwood carbonate (25-μm diameter) and hydrate (2.5-μm diameter): experimental data compared with model predictions.

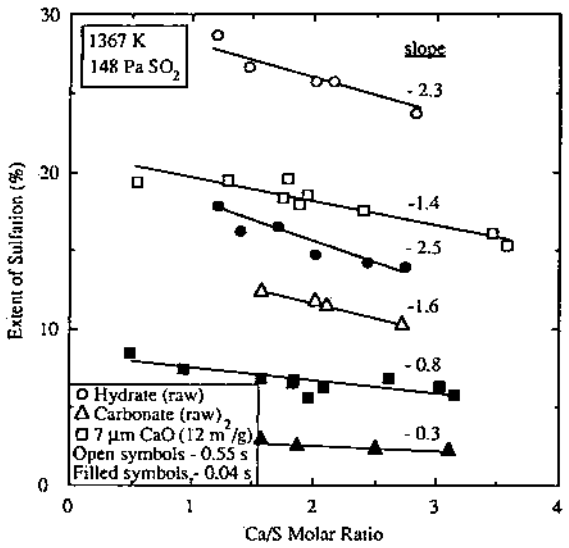

Figure 19. Experimental data for the extent of Ca sulfation as a function of molar Ca/S ratio for Linwood base sorbents.

increased SO_2 concentration for hydrates and carbonates is similar to that observed for precalcines, Figure 10. Note that early capture data (low extent of sulfation) are quite insensitive to an increase in SO_2 partial pressure above 20 Pa. In contrast, the 0.5-s capture data (higher extent of sulfation) show significant increases with rising partial pressure. Thus, there is an apparent increase in reaction order with extent of sulfation.

The model predicts this variability in the SO_2 concentration dependence for different extents of sulfation by assuming that initial sulfation of CaO, until a monolayer of $CaSO_4$ covers the individual grains, is instantaneous and limited only by gas-phase diffusion, and subsequent sulfation, after monolayer coverage, is limited by pore diffusion and product-layer diffusion with an effective reaction order of 0.6 (Milne et al., 1990a). Though the absolute value of the model capture has only fair agreement with the data, the predictions for relative changes in capture with increasing SO_2 concentration are in close agreement with actual observtions.

The influence of molar Ca/S ratio on the extent of sulfation is a result of the concentration dependence al-

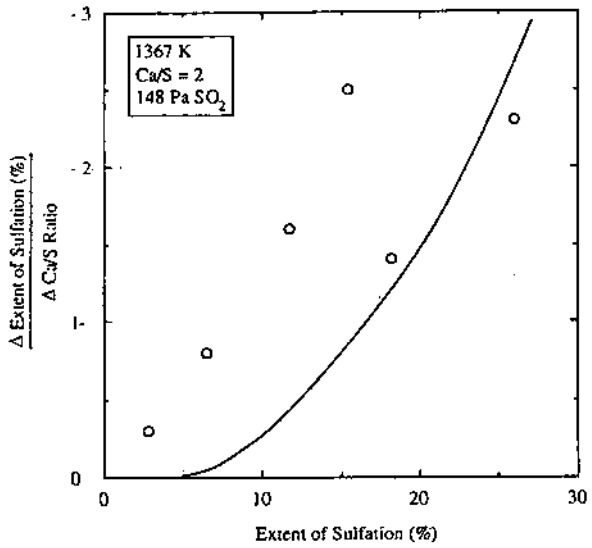

Figure 20. Experimental data and model predictions showing increasing slope of the extent of sulfation (%) versus Ca/S ratio lines with increasing extent of sulfation.

ready discussed. The data of Figure 19 show that, for a given reaction time, the extent of sulfation increases approximately linearly as Ca/S ratio decreases. It is further observed that the slope of these lines generally increases with the extent of sulfation. Model predictions produce this same trend, Figure 20, though the values of the predicted slope are less than the measured values. The diminishing extent of sulfation of the particle with increasing Ca/S ratio results from the fact that, at high ratios, the higher capture results in a lower gas-phase concentration of SO_2 for a given extent of sulfation and thus a lower rate of sulfation. The model predictions indicate that the plot of the extent of sulfation versus Ca/S ratio is slightly concave down rather than linear.

A basic assumption of the theoretical model is that O_2 concentration variations over the range of interest for dry sorbent injection (>3% O_2) do not alter the sulfation rate. Experimental data confirmed this assumption by showing that a 20% change in O_2 partial pressure did not affect the sulfur capture.

Sintering Rate. The influence of increased sintering rates at elevated temperatures is observed in the data and model predictions of Figures 9, 16, and 17. Based on the previous discussion on the influence of SO_2 concentration, it is concluded that sintering is the major factor in causing the asymptotic curves for the capture data at approximately 1447 K. Sintering retards the rate of capture by reducing the CaO surface area and porosity. The impact of the sintering process is illustrated by model predictions that showed 2.5-μm hydrate capture at 0.5 s and 1367 K increasing from 60% with sintering, to 72% without sintering. Predictions on the same basis for 25-μm carbonate revealed an increase from 15% to 19% capture. Thus, sintering has the greatest influence on sulfation that is more strongly limited by product-layer diffusion than by pore diffusion.

Product-Layer Diffusivity. The value of the product-layer diffusivity has the greatest influence on the sulfation rate of small particles where pore diffusion limitations are less dominant. For 25-μm carbonate at 1367 K, model calculations indicated that a 10-fold increase in the product-layer diffusivity resulted in a negligible increase in the level of capture. In contrast, the same 10-fold increase for 2.5-μm hydrate resulted in the capture at 0.5 s rising from 60% to 69%.

Influence of High Mass-Transfer Rates. External heat- and mass-transfer coefficients for a spherical solid surrounded by gas, developed with the assumption of a stagnant gas, can predict incorrect transfer rates when high mass-transfer rates make bulk flow effects significant. The simultaneous calcination and sulfation process merits investigation to see if such high mass-transfer effects are important, but model predictions validated the simpler approach of using Sherwood and Nusselt numbers of 2 to calculate external heat- and mass-transfer coefficients.

Heat Transfer. For the small particles employed in this study, radiation accounts for a small fraction of the heat transfer; neglecting the radiation term of eq 5 resulted in a less than 5 K variance in the calculated temperatures for 10-μm particles injected in a 1367 K gas stream.

The external heat-transfer coefficient is inversely proportional to the particle diameter, eq 2; therefore, heat-transfer limitations are most apparent with the larger particles that also have higher thermal capacities. The more endothermic carbonate decomposition will result in a higher influence of heat-transfer limitations on the sulfation of carbonate particles. Model predictions for the 4.4, 8.9, 21, and 54-μm carbonate particles of this study, injected in a 1367 K, SO_2 laden gas stream showed that the particles temperatures rise from 298 K to 1366, 1364, 1358, and 1266 K, respectively, 0.025 s after injection. For a 25-μm carbonate, the approximation of isothermal reaction at 1367 K versus the nonisothermal reaction including heat transfer showed little change in the predicted sulfation levels with time.

Though the rate of heating as sorbent injection conditions is not negligible on the time scale of dry sorbent injection for particles larger than 10 μm, the influence of the reduced rate of heat transfer is dampened by increasing dominance of pore diffusion at larger particle sizes. Earlier, under the Influence of Calcination Rate section, it was shown that an increase in 25-μm carbonate calcination rate of 37 times, the equivalent rate of hydrate calcination for the same size particle, increased the capture at 0.5 s from 15% to 16%. It was also shown that early capture increases due to accelerated calcination rates are subsequently negated at long times due to the synergistic effect of calcination and sintering. Thus, the approximation of isothermal reaction for model predictions is valid for particles smaller than 10 μm and for larger particles with reaction times longer than 0.2 s.

Sorbent Mixing in the Reactor. Shown in Figure 21 are data for the sulfation of Linwood hydrate at 1373 K measured under different sorbent entrainment conditions. The measurements made for this study were conducted with an efficient four-hole injector nozzle and with single-hole hole nozzle to induce slow mixing of the sorbent jet stream with the reactor gas. The ITR reactor of Newton and Kramlich (1987) had a similar mixing system with a four-hole nozzle injecting the sorbent jet stream into the venturi of the reactor. The STR reactor of Newton and Kramlich had a six-hole injector nozzle without the venturi to facilitate mixing in the reactor. Of most significance in this plot are the variations in shape of the capture curves for the different mixing conditions. For the measurements of this study, the slow mixing conditions reduced capture at a given time. However, slow mixing shows a steeper slope than the four-hole nozzle. For long times, it appears that the two curves merge. A similar pattern is observed when comparing the ITR and STR reactors, but comparison of these two reactors with the four-hole nozzle of this study reveals an additional variation in the curve shape.

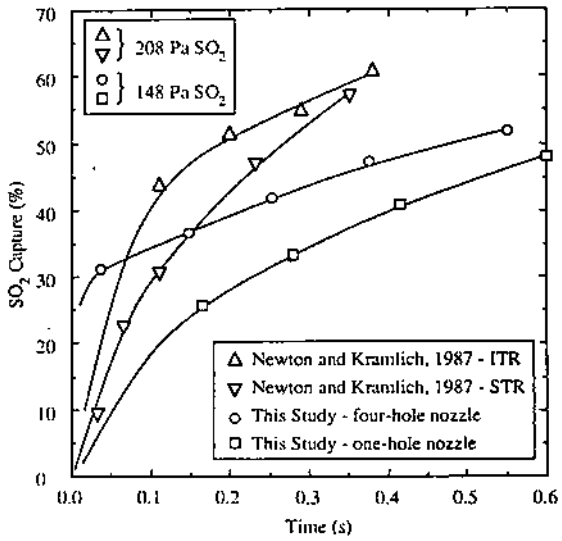

Figure 21. Sulfation data for Linwood hydrate at 1373 K for different reactor mixing conditions.

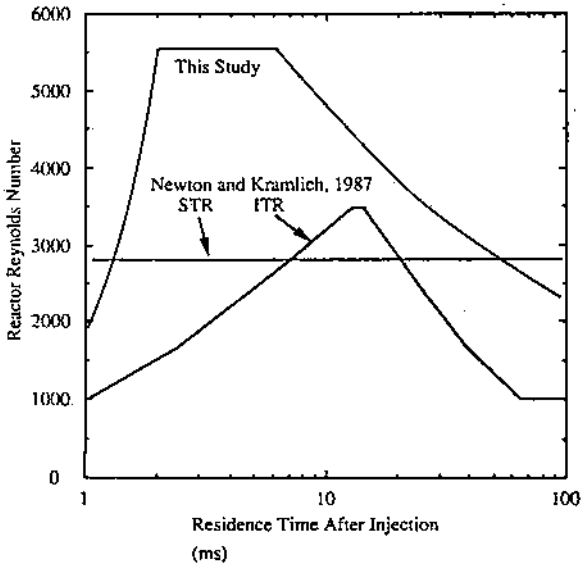

Figure 22. Reactor Reynolds number as a function of sorbent residence time for three isothermal dispersed-phase reactors.

Figure 22 shows the Reynolds number as a function of sorbent residence time in these three reactors. Obviously, the reactors have much different fluid mechanics for mixing the sorbent injection jets and the reactor gas stream. In contrast to its lower capture levels, the reactor of this study exhibits higher levels of turbulence for longer duration than either the ITR reactor or STR reactor. These observations cannot be attributed simply to incomplete mixing; the exact reason for the mixing dependence is elusive. However, the model sheds some light on the hypothesis that mixing conditions can alter the shape of the capture curve and not just shift the curve in time.

Shown in Figure 23 are model predictions for 2.5-μm hydrate at 1367 K with 0-, 0.1-, and 0.2-s mixing times. The complex three-dimensional fluid mechanics of the injector streams mixing with the reactor gas are not modeled; instead, the approximation is made that the concentration of SO_2 and gas temperature immediately surrounding the particles increase linearly through the mixing period. The model predictions indicate that the shape of the capture curve is a function of mixing time. This dependence results from early calcination of the hydrate particles prior to complete mixing. CaO produced at the lower temperatures does not sulfate as rapidly, but

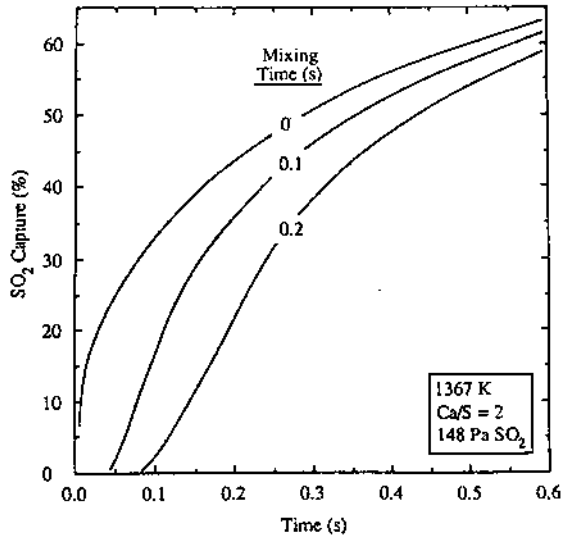

Figure 23. Model prediction of the influence of mixing time assuming linear increase in temperature and concentration through the mixing period for 2.5-μm hydrate.

the high surface area CaO does not sinter as rapidly as at higher temperatures either. Apparently, the lower sintering rate is more significant than the reduced product-layer diffusion rate. For the 0.1-s mixing delay, the time to reach 50% SO_2 capture after complete mixing is 11% less than that for instantaneous mixing. For the 0.2-s mixing delay, this time is reduced by 20%. Model predictions for small $CaCO_3$ particles show a similar mixing dependence but to a lesser extent. The overall influence of the mixing delay in the model predictions is to allow more efficient SO_2 penetration into the particle interior prior to sintering induced deactivation.

These model predictions are based on just a few of the multiple reactions that could take place during particle heating. Bortz et al. (1986) reported that, for 700–923 K, SO_2 reacts directly with $Ca(OH)_2$, without the calcination step, to form $CaSO_3$ and $CaSO_4$. In this temperature range, SO_2 reacts very slowly with CaO, but with $Ca(OH)_2$ they reported 30% conversion to $CaSO_x$ within 0.1 s. They also reported a competing reaction of CO_2 with $Ca(OH)_2$ to form $CaCO_3$. This second reaction becomes dominant at the upper end of this temperature range. These researchers theorized that this low-temperature direct sulfation of $Ca(OH)_2$ has a very high intrinsic rate and that the rate of sulfation is limited by diffusion of SO_2 to the particle from the bulk gas phase. By comparison, Snow et al. (1988) reported direct sulfation of $CaCO_3$ at 1123 K. The calcination reaction of $CaCO_3$ is much faster so a high concentration of CO_2 is essential to allow the direct sulfation to take place. Therefore, direct sulfation of $CaCO_3$ under sorbent injection conditions is not likely.

Consequently, the influence of jet mixing on the sulfation of calcium-based sorbents [primarily $Ca(OH)_2$] injected in a high-temperature combustion gas containing SO_2 cannot be accurately examined without accounting for the multiple reactions that potentially occur at the short times involved in mixing.

Conclusions

The experimental data of this study confirmed that, even when derived from the same parent limestone, hydrated sorbents are clearly superior to carbonate sorbents with respect to SO_2 capture. This difference is primarily attributable to a dramatic difference in prompt SO_2 capture that occurs in the first 0.03 s after injection. Data obtained with narrow size fractions from both the carbo-

nate and hydrate sorbents suggest that the difference in prompt capture is primarily associated with differences in inherent particle size distribution between the two sorbents. The hydration process itself reduces the mean particle size, resulting in a significant increase in the early capture.

The data also suggest that the large decrease in initial sulfur capture with increasing particle size appears to be primarily the result of initial pore diffusion effects because both raw and precalcined sorbents gave similar results. Beyond approximately 0.2 s, the sulfation rate appears to be relatively insensitive to particle size, but the rate of SO_2 capture increase with hydrated sorbent is larger than that measured with the carbonate sorbent. This difference is primarily attributed to the higher initial porosity of the hydrate, before calcination. A significant difference in the pore shape of hydrate- and carbonate-derived CaO is not supported by SEM photomicrographs of high-temperature calcines nor is it necessary to predict the variations observed in the high-temperature sulfur capture data.

It is now well established that the rate of hydrate calcination greatly exceeds that of carbonates, but the sulfur capture data suggest that overall sulfation rate of particles smaller than approximately 5 μm in mean diameter is not limited by calcination. For carbonate particles larger than 10 μm, the calcination delay appears to retard the initial capture, but model predictions indicate that ultimate capture may be only slightly influenced by the calcination delay. On the basis of the viewpoint of the model, the calcination delay postpones the sintering of interior CaO through the period of high reactivity of the exterior shells of the particle. By the time the interior shells of the particle are calcined and available for sulfation, the exterior shells are partially deactivated by product-layer buildup, allowing for better penetration of SO_2 into the particle interior.

On the basis of the data, the optimum isothermal injection temperature appears to be approximately 1400 K. Model predictions indicate a lower value of 1340 K due to a higher retardation of the sulfation rate from higher SO_2 equilibrium concentrations at elevated temperatures than the capture data support. The sintering model developed from the low-temperature differential reactor data of Borgwardt (1989) appears to adequately deactivate the high surface area CaO from calcination to simulate temperature trends in the sulfur capture data of this study.

The theoretical model shows reasonable agreement with the capture trends measured experimentally and is reliable in predicting the relative changes in capture due to changes in SO_2 concentration. This agreement with the data illustrates that the product-layer-diffusion model developed from the low-temperature differential reactor data of Borgwardt and Bruce (1986) extrapolates to high-temperature, short-time conditions experienced in dry sorbent injection.

The inability of the model to predict prompt capture levels measured in the laboratory may be due, in part, to the inappropriate simulation of the irregular particle as a sphere. The same reasoning partially explains the model's subsequent overestimation of the influence of particle size on ultimate capture. The injection of precalcines of known pore structure to obtain fundamental sulfation rate data by which the pore diffusion model could be calibrated proved ineffective due to alteration of the CaO structure from the rapid heating that occurred upon injection.

The influence of high mass-transfer rates on heat- and mass-transfer coefficients for model calculations can be neglected. Furthermore, the influence of heat-transfer limitations for larger particles (>10 μm) is partially negated by the dominance of pore diffusion; therefore, the approximation of isothermal reaction is valid for most conditions with reaction times in excess of 0.2 s.

The effect of sorbent mixing conditions in the reactor cannot be neglected in evaluating short-time, high-temperature sulfation data because of the multiple, rapid reactions that occur while the particle heats to reactor gas temperatures. Model predictions and experimental data indicate that prolonged mixing times do not simply shift the capture curve but result in a differently shaped curve.

The model predictions suggest that the rate of SO_2 capture from the injection of commercial hydrate sorbents in utility boilers should be limited by pore diffusion, product-layer diffusion, and sintering.

Acknowledgment

We gratefully acknowledge the U.S. EPA's extensive financial support and continuing technical assistance throughout the project. This work was also sponsored in part by the Advanced Combustion Engineering Research Center. Funds for this Center are received from the National Science Foundation, the State of Utah, 25 industrial participants, and the U.S. Department of Energy. We also thank Tom Bush of the Linwood Mining and Minerals Corporation for providing the limestone and hydrated lime used in this study.

Nomenclature

a_i, b_i, c_i, d_i, e_i = heat capacity or heat of reaction coefficients for species i
C_{pi} = mean molar heat capacity of gas species i or heat capacity of solid i (J/(kmol K))
F_i = flux of gas species i at the particle surface (kmol/(m^2 s))
h = convective heat-transfer coefficient (W/(m^2 K))
ΔH_{ri} = heat of reaction of reaction i (J/kmol)
k_h = gas mixture thermal conductivity (W/(m K))
n_{Ca} = moles of Ca per particle (kmol)
r_p = particle radius (m)
Δt = time increment (s)
T = temperature (K)
T_g = bulk gas temperature (K)
T_i = temperature of gas species i (K)
T_p = particle temperature (K)
T_{pl} = particle temperature from previous calculation time step (K)
T_w = reactor wall temperature (K)
x_c = extent of calcination
x_s = extent of sulfation

Greek Letters

α = constant defined by eq 6 (W/(m^2 K))
ϵ = emissivity of CaO (0.27)
σ = Stefan–Boltzmann constant (5.669×10^{-8} W/(m^2 K^4))
ϕ_h = dimensionless term defined in eq 3

Registry No. $CaCO_3$, 471-34-1; $Ca(OH)_2$, 1305-62-0; CaO, 1305-78-8; SO_2, 7446-09-5.

Literature Cited

Attig, R. C.; Sedor, P. Additive Injection for Sulfur Dioxide Control: A Pilot Plant Study. NAPCA (EPA) Report APTD 1176 (NTIS PB226761), Babcock & Wilcox Company, March 1970.

Balzhiser, R. E.; Samuels, M. R.; Eliassen, J. D. *Chemical Engineering Thermodynamics: The Study of Energy, Entropy, and Equilibrium*; Prentice-Hall: Englewood Cliffs, NJ, 1972.

Beittel, R.; Gooch, J. P.; Dismukes, E. B.; Muzio, L. J. Studies of Sorbent Calcination and SO_2-Sorbent Reaction in a Pilot-Scale Furnace. *Proc. 1st Joint Symp. on Dry SO_2 and Simul. SO_2/NO_x Control Technol.*, EPA-600/9-85-020a (NTIS PB85-232353);

EPA: Washington, DC, July 1985; Vol. 1, p 16-1.
Bird, R. B.; Stewart, W. E.; Lightfoot, E. N. *Transport Phenomena*; Wiley: New York, 1960.
Borgwardt, R. H. Kinetics of the Reaction of SO_2 with Calcined Limestone. *Environ. Sci. Technol.* 1970, *4*, 59.
Borgwardt, R. H. CaO Sintering in Atmospheres Containing Water and Carbon Dioxide. *Ind. Eng. Chem. Res.* 1989, *28*, 493–500.
Borgwardt, R. H.; Bruce, K. R. Effect of Specific Surface Area on the Reactivity of CaO with SO_2. *AIChE J.* 1986, *32*, 239.
Bortz, S. J.; Flament, P. Recent IFRF Fundamental and Pilot Scale Studies on the Direct Sorbent Injection Process. *Proc. 1st Joint Symp. on Dry SO_2 and Simul. SO_2/NO_x Control Technol.*, EPA-600/9-85-020a (NTIS PB85-232353); EPA: Washington, DC, July 1985; Vol. 1, p 17–1.
Bortz, S. J.; Roman, V. P.; Yang, R. J.; Offen, G. R. Dry Hydroxide Injection At Economizer Temperatures for Improved SO_2 Control. *Proc. 1986 Joint Symp. on Dry SO_2 and Simul. SO_2/NO_x Control Technol.*, EPA-600/9-86-029b (NTIS PB87-120457); EPA: Washington, DC, Oct 1986.
Boynton, R. S. *Chemistry and Technology of Lime and Limestone*, 2nd ed.; Wiley: New York, 1980.
Coutant, R. W.; Simon, R.; Campbell, B. E.; Barrett, R. E. Investigation of the Reactivity of Limestone and Dolomite for Capturing SO_2 from Flue Gas. NAPCA (EPA) Report APTD 0802 (NTIS PB204385), Battelle Memorial Institute, Oct 1971.
Gambill, W. R. Prediction and Correlation of Physical Properties. In *Chemical Engineers' Handbook*, 5th ed.; Perry, R. H., Chilton, C. H., Eds.; McGraw-Hill: New York, 1973.
Gullett, B. K.; Blom, J. A. Calcium Hydroxide and Calcium Carbonate Particle Size Effects on Reactivity with Sulfur Dioxide. *React. Solids* 1987, *3*, 337.
Gullett, B. K.; Bruce, K. R. Pore Distribution Changes of Calcium-Based Sorbents Reacting with Sulfur Dioxide. *AIChE J.* 1987, *33*, 1719.
Hartman, M.; Coughlin, R. W. Reaction of Sulfur Dioxide with Limestone and the Grain Model. *AIChE J.* 1976, *22*, 490.
Holman, J. P. *Heat Transfer*, 4th ed.; McGraw-Hill: New York, 1976.
Hougen, O. A.; Watson, K. M.; Ragatz, R. A. *Chemical Process Principles: Part I. Material and Energy Balances*, 2nd ed.; Wiley: New York, 1954.
Ishihara, Y. Kinetics of the Reaction of Calcined Limestone with Sulfur Dioxide in Combustion Gases. Presented at the Dry Limestone Injection Process Symposium, Gilbertsville, KY, June 22–26, 1970.
Liley, P. E. Physical and Chemical Data. In *Perry's Chemical Engineers' Handbook*, 6th ed.; Perry, R. H., Green, D. W., Eds.; McGraw-Hill: New York, 1984.
Lindner, B.; Simonsson, D. Comparison of Structural Models for Gas–Solid Reactions in Porous Solids Undergoing Structural Changes. *Chem. Eng. Sci.* 1981, *36*, 1519.
Milne, C. R.; Silcox, G. D.; Pershing, D. W.; Kirchgessner, D. A. Calcination and Sintering Models for Application to High-Temperature, Short-Time Sulfation of Calcium-Based Sorbents. *Ind. Eng. Chem. Res.* 1990a, *29*, 139–149.
Milne, C. R.; Silcox, G. D.; Pershing, D. W.; Kirchgessner, D. A. High-Temperature, Short-Time Sulfation of Calcium-Based Sorbents. 1. Theoretical Sulfation Model. *Ind. Eng. Chem. Res.* 1990b.
Newton, G. H.; Kramlich, J. C. private communication, 1987.
Overmoe, B. J.; Chen, S. L.; Ho, L.; Seeker, W. R.; Heap, M. P.; Pershing, D. W. Boiler Simulator Studies on Sorbent Utilization for SO_2 Control. *Proc. 1st Joint Symp. on Dry SO_2 and Simul. SO_2/NO_x Control Technol.* EPA-600/9-85-020a (NTIS PB85-232353); EPA: Washington, DC, July 1985; Vol. 1, p 15-1.
Reid, W. T. Basic Factors in the Capture of Sulfur Dioxide by Limestone and Dolomite. *J. Eng. Power, Trans. ASME* 1970, Jan.
Satterfield, C. N.; Feakes, F. Kinetics of the Thermal Decomposition of Calcium Carbonate. *AIChE J.* 1959, *5*, 115.
Silcox, G. D.; Chen, S. L.; Clark, W. D.; Kramlich, J. C.; LaFond, J. F.; McCarthy, J. M.; Pershing, D. W.; Seeker, W. R. Status and Evaluation of Calcitic SO_2 Capture: Analysis of Facilities Performance. EPA-600/7-87-014 (NTIS PB87-194783); EPA: Washington, DC, May 1987.
Slaughter, D. M.; Silcox, G. D.; Lemieux, P. M.; Newton, G. H.; Pershing, D. W. Bench Scale Evaluation of Sulfur-Sorbent Reactions. *Proc. 1st Joint Symp. on Dry SO_2 and Simul. SO_2/NO_x Control Technol.*, EPA-600/9-85-020a (NTIS PB85-232353); EPA: Washington, DC, July 1985; Vol. 1, p 11-1.
Snow, M. J. H.; Longwell, J. P.; Sarofim, A. F. Direct Sulfation of Calcium Carbonate. *Ind. Eng. Chem. Res.* 1988, *27*, 268.

Received for review January 12, 1990
Revised manuscript received May 21, 1990
Accepted July 11, 1990